World Academy of Science, Engineering and Technology
International Journal of Biomedical and Biological Engineering
Vol:6, No:5, 2012

Basic Research for Distinguishing Small Retinal Hemorrhages from Dust Artifact by using Hue, Lightness, and Saturation Color Space

Naoto Suzuki

Abstract**—**To distinguish small retinal hemorrhages in early diabetic retinopathy from dust artifacts, we analyzed hue, lightness, and saturation (HLS) color spaces. The fundus of 5 patients with diabetic retinopathy was photographed. For the initial experiment, we placed 4 different colored papers on the ceiling of a darkroom. Using each color, 10 fragments of house dust particles on a magnifier were photographed. The colored papers were removed, and 3 different colored light bulbs were suspended from the ceiling. Ten fragments of house dust particles on the camera's object lens were photographed. We then constructed an experimental device that can photograph artificial eyes. Five fragments of house dust particles under the ocher fundus of the artificial eye were photographed. On analyzing HLS color space of the dust artifact, lightness and saturation were found to be highly sensitive. However, hue was not highly sensitive.

Keywords**—**Dust artifact, HLS color space, Retinal hemorrhage, and Diabetic retinopathy

I. Introduction

IN Japan, the number of patients with diabetes is increasing along with the rising number of patients with life-style related diseases. According to national research results from the Ministry of Health, Labor, and Welfare in 2005, the number of Japanese patients with diabetes was 16.2 million [1]. They estimated that the number would be 19.0 million in five years. Diabetes is affecting an increasing number of patients, causing complications for eyes, kidneys, and nerves. Many patients with diabetic retinopathy [2] must go to the doctors to prevent blindness [3]-[5]. Early diagnosis is very important [6]; however, detection of small retinal hemorrhages in patients with cloudy ocular media, such as a cataract, is difficult because many hemorrhages are minuscule [7],[8]. Moreover, as shown in Fig. 1, magnified images taken with a fundus camera can be unclear.

A picture taken of several house dust particles flying around in a room would have a number of white spots on it [9],[10].The flash reflecting from house dust particles causes these white spots. Fig. 2 shows the theory of the creation of these spots. Many of the house dust particles are out of focus, and the flash reflected from the house dust is stronger than that reflected from more distant objects. These white spots are called dust artifacts [11]-[13]. If some dust is on the camera's object lens, the reflected light from the objects is obscured by dust particles, and black spots appear in the pictures. These black spots are also called dust artifacts.

N. Suzuki is with Hiroshima International University, Higashi-Hiroshima, Hiroshima 7392695 Japan (phone: 81-823-70-4593; fax: 81-823-70-4542; e-mail: n-suzuki@ hs.hirokoku-u.ac.jp).

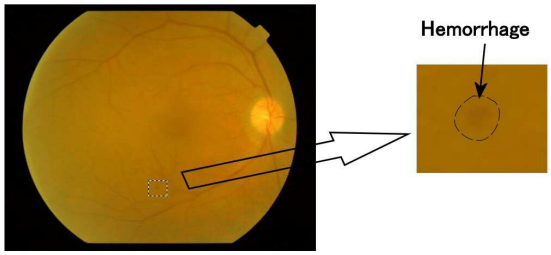

Fig. 1 The area of small retinal hemorrhage in the fundus image of patient with diabetic retinopathy

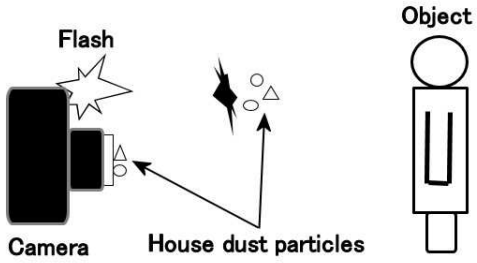

Fig. 2 The light from the flash reflected by dust particles and covered by dust

Fig. 3 shows the basic optical system of a fundus camera [14],[15]. If house dust sticks to the lens, the fundus photographs will contain dust artifacts.

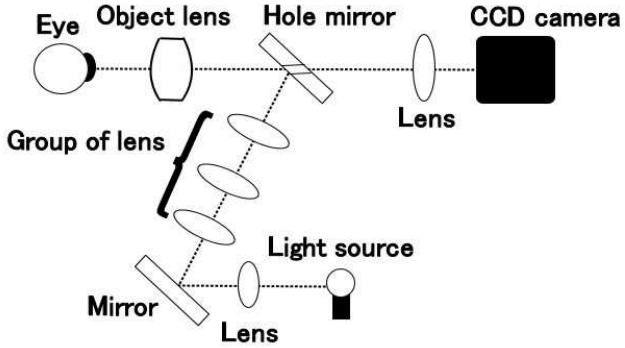

Fig. 3 Basic optical system of the fundus camera

We investigated the research papers on a dust artifact [16]-[18]. Previously, two methods of image clarification have been explored: deleting dust artifacts from images and removing house dust from parts of the device. However, these studies did not investigate the possible medicinal applications of such image clarification [11], [19]-[23]. On the other hand, one researcher explored image artifacts other than dust artifacts,

using image processing to delete some image artifacts from photographs. And another investigated how the image artifacts enter into the fundus photographs [24]-[26]. No one has theoretically examined the effect of flash photos taken in the presence of airborne dust, nor conducted basic research on the light transparency of house dust particles. The cause of white and black spots on photographs must be determined. We performed a basic experiment to photograph white and black spots and examined their influence on the ability of computers to distinguish small retinal hemorrhages in diabetic retinopathy from dust artifacts. Furthermore, to examine the possible clinical applications of our findings, we performed an experimental involving dust artifact photography using an artificial eye.

Small hemorrhages in diabetic retinopathy are distinguished from dust artifacts by using the color space in a fundus photograph [27]. A dust artifact is caused by the diffused reflection of house dust and covering of flash light. This dust artifact is reflected brightly by diffused reflection and is darkly reflected by covering of light. Therefore, the most important element in the concept of color space is lightness. House dust is complicated in form and uneven in density. Light volume is irregular due to the diffuse reflection. Dust artifacts create a spotty pattern. The second most important element is the concentration of color. In diabetic retinopathy, the fundus is reddish-brown or yellow in color. Therefore, in this study, red, brown, ocher, yellow black colors were investigated. The CIE and Munsell color systems can be used to define colors in a color space [28]. The CIE color system characterized many color spaces, including RGB, XYZ, and Lab [28]. The RGB color space has three primary colors: red, green, and blue. Because the color of fundus is closer to red, it is possible to use this color space, although it is difficult to judge lightness and concentration of color. As for the XYZ color space, Y expresses lightness, Z expresses the degree of blueness, and X expresses other elements. Y, corresponding to lightness, can be used for dust artifact detection. Because fundus color is near red, X may be usable. The L of the Lab color space expresses lightness and can be used for distinction. Both “a” and “b” represent the complementary colors. “a” represents the color between red, magenta and green. “b” represents the color between yellow and blue. When both “a” and “b” are used, they may be able to identify fundus color. However, there is no means by which the concentration of a color is distinguishable from other colors. The Munsell color system uses the HLS (hue, lightness, and saturation) color space. Lightness can be used. Since saturation is a numerical value showing the concentration of a color, it is easy to use. The intermediate color between red and yellow is orange. Considering that dark orange resembles brown, it is easy to judge the range of red, brown, and yellow using a hue circle. Therefore, we adopted the HLS color space in our study.

II. Purpose

To distinguish the small retinal hemorrhages in early diabetic retinopathy from dust artifacts, we analyzed the hue, lightness, and saturation (HLS) color spaces [29]-[31]. First, we performed an experiment using 3 colored light bulbs and a magnifier to investigate the influence of white and black spots. To apply the concept of HLS color space to ophthalmologic diagnosis, we performed an experiment involving photography of an artificial eye.

III. Methods

A. Method for distinguishing small retinal hemorrhages from dust artifacts using the HLS color space

The upper side of Fig. 4 shows the division of the fundus image into the hemorrhagic area and the area around the hemorrhage. Paint Shop Pro v. 8.0 was used to visualize the HLS color spaces of these four areas, and the RGB values were transformed from the fundus image to the HLS color space. The hue, lightness, and saturation values ranged from 0 to 255. Hue is the actual color and value is the number assigned on the color wheel (red = zero, yellow = 43, green = 85, cyan = 128, blue = 170, and magenta = 212). Lightness is the brightness of the hue (zero = black, 128 = middle grey, and 255 = white). Saturation is the level of grey added to the hue (zero = very grey and unsaturated and 255 = no grey and fully saturated) [32]. Equation (1) shows the average color space of the hemorrhagic area, **avehm**, and (2) shows the average color space of the area around hemorrhage, **aveahm**.

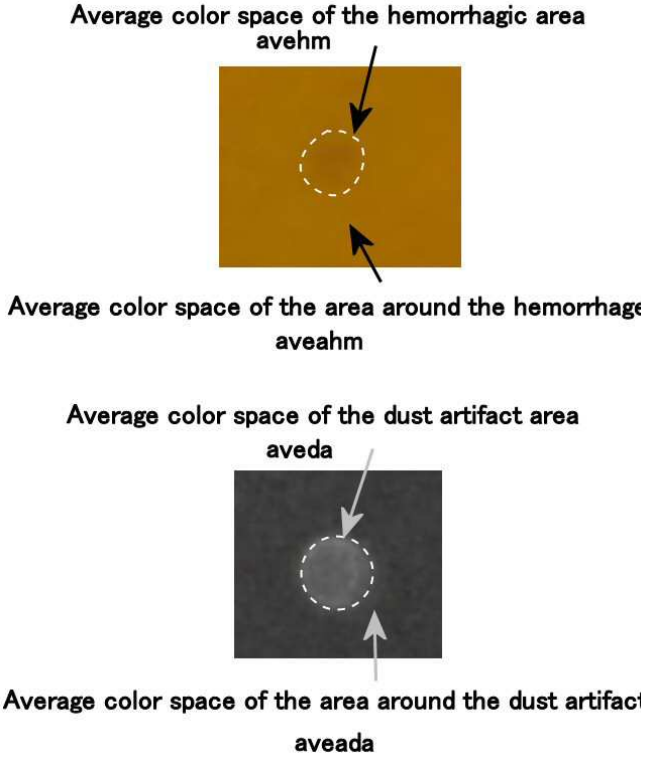

Fig. 4 The average color space of both the hemorrhagic area and the area around the hemorrhage (up), and the average color space of the dust artifact area and the area around the dust artifact (down)

$$\mathbf{avehm} = \begin{bmatrix} AveH\_hm \\ AveL\_hm \\ AveS\_hm \end{bmatrix} \quad (1)$$

$$\mathbf{aveahm} = \begin{bmatrix} AveH\_ahm \\ AveL\_ahm \\ AveS\_ahm \end{bmatrix} \quad (2)$$

The lower side of Fig. 4 shows the division of the image between the dust artifact area and the area around the dust artifact. Paint Shop Pro was used to visualize the HLS color spaces of both these areas. (3) shows the average color space of the dust artifact area, **aveda**, and (4) shows the average color space of the area around dust artifact, **aveada**.

$$\mathbf{aveda} = \begin{bmatrix} AveH\_da \\ AveL\_da \\ AveS\_da \end{bmatrix} \quad (3)$$

$$\mathbf{aveada} = \begin{bmatrix} AveH\_ada \\ AveL\_ada \\ AveS\_ada \end{bmatrix} \quad (4)$$

The hue is generally expressed using 360° of a color circle [31]-[33]. The average degrees of hue related to a hemorrhage are expressed by **AveHD_mh** and **AveHD_amh**. The average degrees of the hue related to a dust artifact are expressed by **AveHD_da** and **AveHD_ada**. (5) to (8) show these average degrees of hue.

$$AveHD\_hm = \frac{AveH\_hm}{255} \cdot 360° \quad (5)$$

$$AveHD\_ahm = \frac{AveH\_ahm}{255} \cdot 360° \quad (6)$$

$$AveHD\_da = \frac{AveH\_da}{255} \cdot 360° \quad (7)$$

$$AveHD\_ada = \frac{AveH\_ada}{255} \cdot 360° \quad (8)$$

(9) to (12) show the average color spaces, **AveHm**, **AveAhm**, **AveDa,** and **AveAda** using the average degrees of hue.

$$\mathbf{AveHm} = \begin{bmatrix} AveHD\_hm \\ AveL\_hm \\ AveS\_hm \end{bmatrix} \quad (9)$$

$$\mathbf{AveAhm} = \begin{bmatrix} AveHD\_ahm \\ AveL\_ahm \\ AveS\_ahm \end{bmatrix} \quad (10)$$

$$\mathbf{AveDa} = \begin{bmatrix} AveHD\_da \\ AveL\_da \\ AveS\_da \end{bmatrix} \quad (11)$$

$$\mathbf{AveAda} = \begin{bmatrix} AveHD\_ada \\ AveL\_ada \\ AveS\_ada \end{bmatrix} \quad (12)$$

DiffH_hm is the difference between the average degrees of hue in the hemorrhage area and the average degrees of hue in the area around the hemorrhage. **DiffH_da** is the difference between the average degrees of hue in the dust artifact area and the average degrees of hue in the area around the dust artifact. **CngL_hm** is the rate of change in lightness of the hemorrhage area to the lightness of the area around the hemorrhage. **CngS_hm** is the rate of change in the saturation of the hemorrhage area to the saturation of the area around the hemorrhage. **CngL_da** is the rate of change in lightness of the dust artifact area to the lightness of the area around the dust artifact. **CngS_da** is the rate of change in the saturation of the dust artifact area to the saturation of the area around the dust artifact. (13) shows the color space change in the hemorrhage area, **CngHm**, and (14) shows the color space change in the dust artifact area, **CngDa**.

$$\mathbf{CngHm} = \begin{bmatrix} DiffH\_hm \\ CngL\_hm \\ CngS\_hm \end{bmatrix} = \begin{bmatrix} 1 & 0 & 0 \\ 0 & 1/AveL\_ahm & 0 \\ 0 & 0 & 1/AveS\_ahm \end{bmatrix} \times (\mathbf{AveHm} - \mathbf{AveAhm}) \quad (13)$$

$$\mathbf{CngDa} = \begin{bmatrix} DiffH\_da \\ CngL\_da \\ CngS\_da \end{bmatrix} = \begin{bmatrix} 1 & 0 & 0 \\ 0 & 1/AveL\_ada & 0 \\ 0 & 0 & 1/AveS\_ada \end{bmatrix} \times (\mathbf{AveDa} - \mathbf{AveAda}) \quad (14)$$

(15) shows **AveCngHm**, which is the average of **CngHm**.

$$\mathbf{AveCngHm} = \begin{bmatrix} AveDiffH\_hm \\ AveCngL\_hm \\ AveCngS\_hm \end{bmatrix} \quad (15)$$

(16) shows the color space for an evaluation, **Ev**, which is the rate of change of **CngDa** to **AveCngHm**.

$$\mathbf{Ev} = \begin{bmatrix} EvH \\ EvL \\ EvS \end{bmatrix} = \begin{bmatrix} 1/AveDiffH\_hm & 0 & 0 \\ 0 & 1/AveCngL\_hm & 0 \\ 0 & 0 & 1/AveCngS\_hm \end{bmatrix} \times \mathbf{CngDa} \quad (16)$$

B. Fundus photography of the five patients with diabetic retinopathy

Fundus photographs were taken in five patients using the fundus camera Topcon TRC-50EX mydriatic retinal camera with a Nikon digital camera D1x. The image sensor was a 23.7 × 15.6-mm, 12-bit RGB CCD [34]. The file format is JPEG baseline-compliant. The number of recorded pixels is 2000 × 1312. Paint Shop Pro was used to visualize the average color space of the hemorrhagic area, **avehm**, and the average color space of the area around the hemorrhage, **aveahm**, in two locations of the photograph.

C. Photography of dust artifacts using three colored light bulbs

In order to investigate the influence of black spots, the experiment was performed using colored light bulb. In the darkroom, three colors of bulbs (yellow, brown, and red) were suspended from the ceiling of the experimental device (Fig. 5). The camera had a dust particle that was 5 × 5 × 5 mm^3 on the object lens. Using each color of bulb, 10 fragments of house dust particles were photographed. The distance between the camera's object lens and the edge of the light bulb was 50 mm. Paint Shop Pro was used to visualize the HLS color spaces of

the dust artifact area and the area around the dust artifact. We used a FinePix J30 digital camera (Fuji Photo Film Co., Japan) in these experiments. We also used a 1/2.3–in square-pixel charged-coupled device (CCD) with a primary color filter [35]. The file format is Exif 2.2 JPEG (compressed). The number of recorded pixels was 4000 × 3000. Table I shows specifications of the colored light bulbs used in this study.

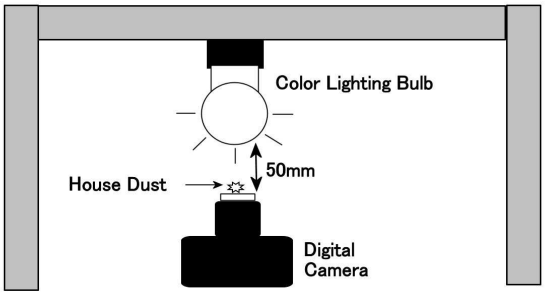

Fig. 5 a diagram of the experimental device taking photos of dust artifacts

TABLE I
SPECIFICATIONS OF THE COLORED LIGHT BULBS

Model	GWR110 V60 WG95K	GWY110 V60 WG95K	Balloon Color G95E26
Maker	TOKI		Kyokko Electric
Color	Red	Yellow	Brown
Cap	E26		
Power	60W		
Voltage	100/110V		
Total length	127mm		124mm
Bulb Sphere	95mm		

D. Photography of dust artifacts using a magnifier

In order to investigate the influence of white spots, the experiment was performed using a magnifier. Fig. 6 shows the experimental device. The darkroom had four colors of papers on its ceiling: red, yellow, brown, and black. The distance between the camera's object lens and the 8-diopter magnifier was 50 mm, and the distance between the magnifier and the ceiling was 485 mm. The magnifier held a dust particle measuring 5 × 5 × 5 mm^3. Using a flash and each color of paper, 10 fragments of dust particles were photographed. The magnifier was a Claire Lupe PB60 (Vixen Co.) and its specifications are shown in Table Ⅱ.

TABLE II
SPECIFICATIONS OF THE MAGNIFIER

Lens diameter	60mm
Diopter	8.0D
Magnification	3.0
Lens material	Acrylic resin
Lens coat	Multi coat with Anti-Reflection coat
Frame material	Acrylonitrile butadiene styrene

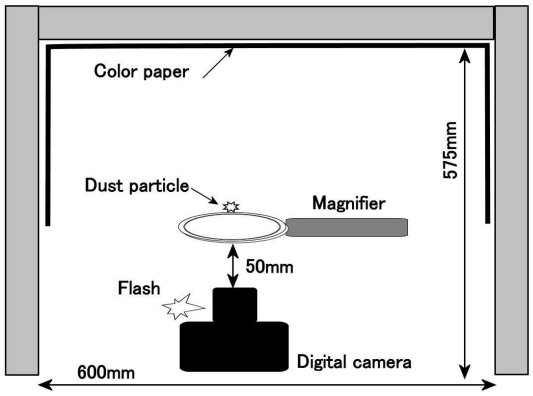

Fig. 6 A diagram of the experimental device taking photos of dust on a magnifier

E. Optical system diagram of the experimental device

We constructed an experimental device to photograph the fundus of artificial eyes. The optical system of this device was same as that of a fundus camera. Therefore, the optical system of the experimental device was analysed using optical design software (OpTaliX-LT 7.11). Fig. 7 shows an illumination optical system and a photographic optical system, including the distance between lenses and the distance between a lens and a mirror per mm. The device consists of a canon EOS 50D camera with an EF 50 mm f/1.8-2 camera lens, a Speedlite 270EX flash, an object lens with 50-mm focal length and a center thickness of 16 mm, four double-convex lenses with focal lengths of 100 mm and center thicknesses of 10 mm, three aperture stops, a mirror with a hole with 4 mm diameter, another mirror, and an artificial eye. The object lens, four double-convex lenses, and two mirrors are all 50 mm in diameter. Fig. 7 shows the aperture stop equipped with a 13-mm-diameter hole on the right side of the device. The hole in the middle aperture stop was 45 mm in diameter. The aperture stop on the left side of the device was equipped with a 39-mm-diameter hole. Three wires hang a black plate 15 mm in diameter in the center of the hole. The axial distance from eyeground to the image surface is 797.3 mm and that from eyeground to the strobe surface is 858.9 mm.

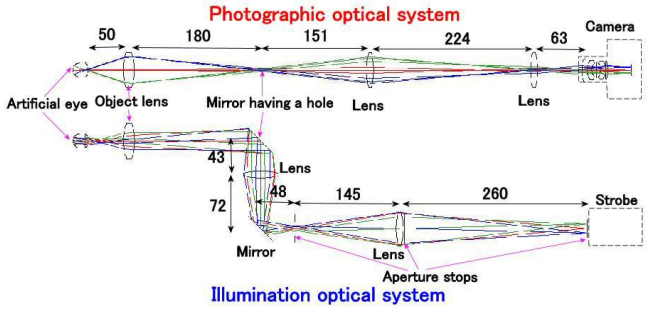

Fig. 7 Optical system diagram of the experimental device

F. Artificial eye

The artificial eye, shown in Fig. 8, consists of a plane-convex lens, a black spacer with a hole 18 mm in diameter, and a hemispherical cup. The plane-convex lens was 20 mm in diameter, with a 4.6-mm center thickness and a 17.4-mm back focal length. The hemispherical cup was 20 mm in diameter with a thickness of 0.5 mm.

The distance from the surface of the plane-convex lens to the eyeground was 22 mm. MgF2 coating was applied to the surface of the plane-convex lens. The hemispherical cup was made of polyethylene terephthalate. Because the fundus color in Fig. 1 resembles ocher, the cup was painted using an ocherous matt color spray (Asahipen Corp., Osaka, Japan). Gold amber was used as ocher.

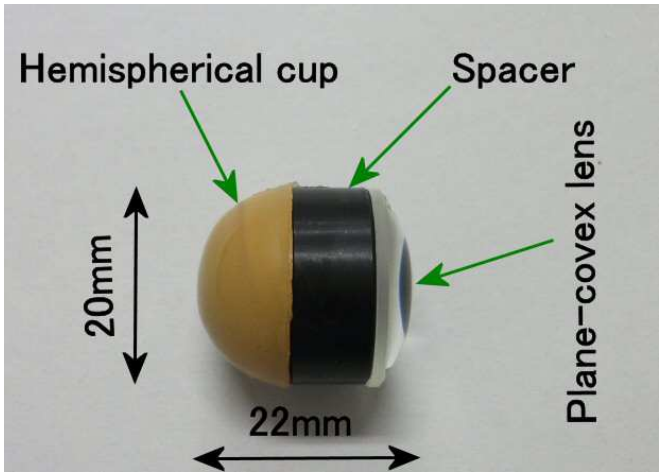

Fig. 8 Artificial eye

G.Experimental device

The experimental device, shown in Fig. 9, was equipped with an illumination optical system and a photographic optical system separated by a mirror with a hole 4 mm in diameter. An MgF2 coating was applied to the surface of all lenses. The image sensor used was a 22.3 × 14.9-mm CMOS sensor [36]. The file format was JPEG, RAW (14-bit Canon original). The number of recorded pixels was 4752 × 3168.

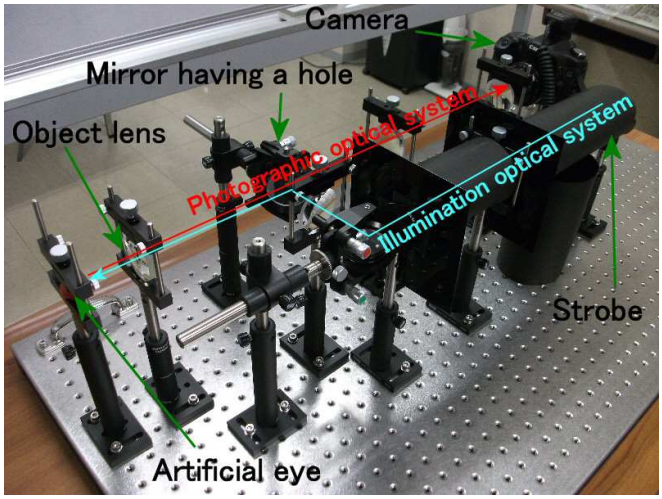

Fig. 9 Experimental device

H.Specimens

We prepared five types of fragments of house dust measuring about 5 × 5 × 5 mm^3. Each fragment was set at the central part and artificial eye side on the object lens. Then fragments were photographed one by one. Paint Shop Pro was used to visualize the HLS color space of four areas, as shown in Fig. 4.

I. Calculation of evaluation space for house dust using HLS data

(16) shows the color space for evaluation (**Ev**), which is the ratio of change of **CngDa** to **AveCngHm**. **CngDa** is the color space change in the dust artifact area and **AveCngHm** is the average of the color space change in the hemorrhage area. The greater the absolute values of **EvH**, **EvL**, and **EvS**, the greater the extent to which the HLS color space can be used to distinguish small hemorrhages from dust artifacts. These absolute values must be > 1.0.

IV. Results

A. The changed color spaces of the hemorrhagic area

Fig. 10 shows 10 images of small retinal hemorrhagic areas clipped from 5 fundus photos. Paint Shop Pro was used to visualize both **avehm** and **aveahm** from the images. The changed color space of the hemorrhagic areas is **CngHm**. **CngHm** was calculated by substituting **avehm** and **aveahm** in (5), (6), (9), (10), and (13). Table Ⅲ shows the average and standard deviation of **CngHm**.

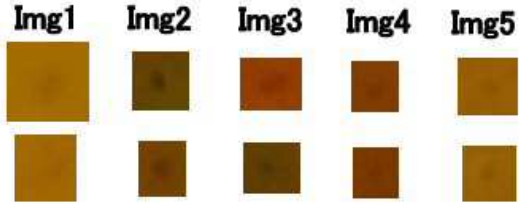

Fig. 10 Ten images of the small hemorrhagic area of patients with diabetic retinopathy

TABLE III
THE CHANGED COLOR SPACE OF THE HEMORRHAGIC AREAS, **CngHm**

Object	Numerical values
DiffH_hm	−1.0°±1.2°
CngL_hm	−0.04±0.02
CngS_hm	−0.01±0.02

B. Dust artifacts photographed under the colored light bulbs

Fig. 11 shows 30 images of dust artifacts clipped from the photos taken by methods *C*.

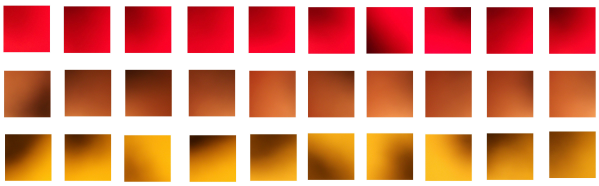

Fig. 11 Thirty images of dust artifacts clipped from the photos taken by method *C*

Paint Shop Pro was used to visualize both **aveda** and **aveada** from 30 images in Fig. 11. **Ev** was calculated by substituting **aveda** and **aveada** for **AveDa** and **AveAda** in (7), (8), (11), (12), (14), (15), and (16). If AveHD_ada was near 360°, we changed AveHD_ada to "AveHD_ada – 360°" to maintain the continuity of the color wheel. We used the preceding methods for AveHD_ada in results *B* and *C*.

To compare the color spaces of the small hemorrhagic areas with the color spaces of the dust artifact areas, Fig. 12 shows both the averages and the standard deviations of EvL values, obtained from photos taken of dust particles under each color of bulb. The averages are shown as both bar graphs and values, and the standard deviations are shown as lines. According to Fig. 12, the average EvL values were brown 5.7, red 6.4, and yellow 10.0. The average CngL_ad values of all colors were 5.7 times more than the AveCngL_hm values. This shows that "|CngL_ad| > |AveCngL_hm|" was consistently dominant. The lightness can be used to distinguish small hemorrhages from dust artifacts.

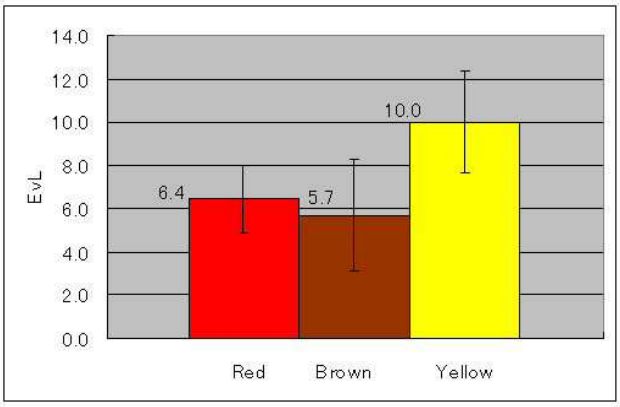

Fig. 12 Variable EvL

According to Table Ⅳ, the average EvH values were red –3.3, brown 1.6, and yellow 7.9. The standard deviation of EvH values for brown was a little large. This shows that "|CngH_da| > |AveCngH_hm|" was consistently dominant, except for brown. The hue can be used to distinguish small hemorrhages from dust artifacts, except for brown. Next, the average EvS values were red 0.9, brown –2.8, and yellow –2.2. The standard deviations of EvS values for all colors were large; thus, saturation cannot be used to distinguish small hemorrhages from dust artifacts.

TABLE IV
VARIABLE EVS AND EVH

Background Color	EvS	EvH
Red	0.9±0.9	−3.3±1.4
Brown	−2.8±9.2	1.6±1.4
Yellow	−2.2±6.6	7.9±1.7

C. Dust artifacts with house dust particles on a magnifier

Fig. 13 shows 40 images of dust artifacts clipped from photos taken by method *D*. Paint Shop Pro was used to visualize both **aveda** and **aveada** from the images in Fig. 13. **Ev** was calculated by substituting these spaces for both **AveDa** and **AveAda** in (7), (8), (11), (12), (14), (15), and (16). Fig. 14 shows the average and the standard deviations of EvL values. The averages are shown as both the bar graphs and values, and the standard deviations are shown as lines**.** Table Ⅴ shows the EvH and EvS values.

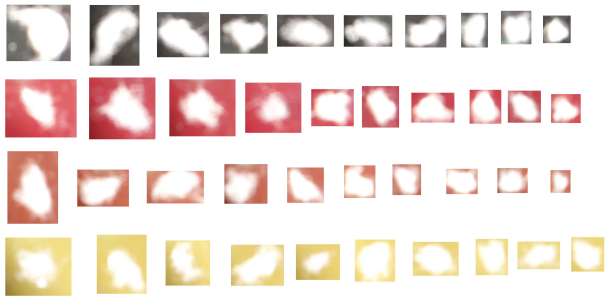

Fig. 13 Forty images clipped from many photos taken by using method *D*

According to Fig. 14, all of EvL values were below zero because AveCngL_hm values were below zero and CngL_ad values were above zero. The absolute values of average EvL were yellow 8.5, brown 11.5, red 14.5, and black 24.0. The greater the absolute values of EvL, the greater the extent to which the HLS color space can be used to distinguish small hemorrhages from dust artifacts. Thus, lightness can distinguish small hemorrhages from dust artifacts.

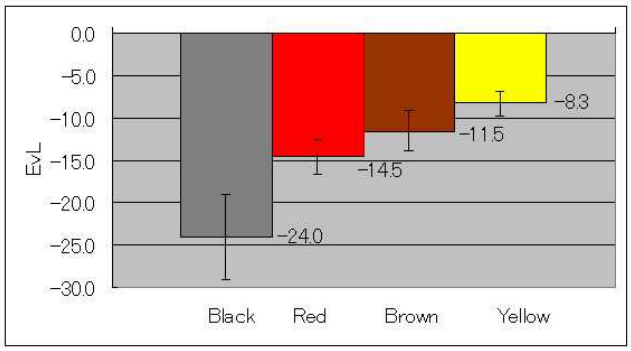

Fig. 14 Variable EvL

TABLE V
VARIABLE EVS AND EVH

Background color	EvS	EvH
Black	−163.8±84.5	52.6±24.8
Red	54.1±32.6	−116.6±33.1
Brown	44.0±27.8	−1.6±6.3
Yellow	45.6±21.6	16.9±4.1

According to Table Ⅴ, |CngS_da| values were very large if the background color was black or yellow, and "|CngS_da| > |AveCngS_hm|" held true. Their standard deviations were a little large, but that presented no problem. If the background color is black or yellow, saturation can distinguish small hemorrhages from dust artifacts; however, if the background color is red or brown, saturation cannot distinguish small hemorrhages from dust artifacts because their standard deviations are large. On the other hand, if the background color is black, red or yellow, the |CngH_da| values are very large, and "|CngH_da| > |AveCngH_hm|" holds true. Their standard deviations were not large, and presented no problem. If the background color is black, red or yellow, hue can distinguish small hemorrhages from dust artifacts; however, when the

background color is brown, the hue cannot distinguish small hemorrhages from dust artifacts because of the large standard deviations.

D.Changed color spaces of the dust artifact area

The ocher fundus of the artificial eye was photographed 5 times with a fragment of house dust set on the central part and artificial eye side of the object lens. Fig. 15 shows 5 images of dust artifact areas.

Fig. 15 Five images of the dust artifact areas clipped from the artificial eye photographs

E. Evaluation space for house dust on the object lens under the artificial eye

Table VI shows averages and standard deviations of the **EvL**, **EvS**, and **EvH** values. These values are obtained from photographs of dust particles on the object lens. As seen in Table VI, the average **CngL_da** value was 9.5 times higher than the **AveCngL_hm** values, indicating that "|**CngL_da**| > |**AveCngL_hm**|" was consistently dominant. Therefore, lightness can be used to distinguish small hemorrhages from dust artifacts. In addition, the average **CngS_da** value was 5.0 times higher than the **AveCngS_hm** values, indicating that "|**CngS_da**| > |**AveCngS_hm**|" was consistently dominant. Thus, saturation can also be used to distinguish small hemorrhages from dust artifacts. However, the average **CngH_da** value was lower than the **AveCngH_hm** values, indicating that "|**CngH_da**| > |**AveCngH_hm**|" was not consistently dominant. Therefore, it is difficult to distinguish small hemorrhages from dust artifacts on the basis of hue.

TABLE VI
VARIABLE EvL, EvS, AND EvH

EvL	EvS	EvH
9.5±1.8	5.0±2.8	0.3±2.3

V. DISCUSSION

A. The relation among four background colors

Fig. 16 shows the relation of hue to lightness for four of the background colors used in the experiment. In reporting the experimental results in Tables Ⅶ to Ⅸ, we used "T" if the indices could distinguish hemorrhages from dust artifacts, and "F" if not; we used "M" to indicate that indices could distinguish hemorrhages from dust artifacts with some conditions. For example, if the background color is red or yellow and if the index can distinguish hemorrhages from dust artifacts, then both segments 1 and 4 are "T." Segment 1 is "M" and segment 4 is "F" if the index can make the distinction when the background color is red but not when the background color is yellow. Segment 1 is "F" and segment 4 is "M" if the index cannot make the distinction when the background color is red, but it can if the background color is yellow. Both segments 1 and 4 are "F" if the index cannot make that distinction when the background colors are either red or yellow.

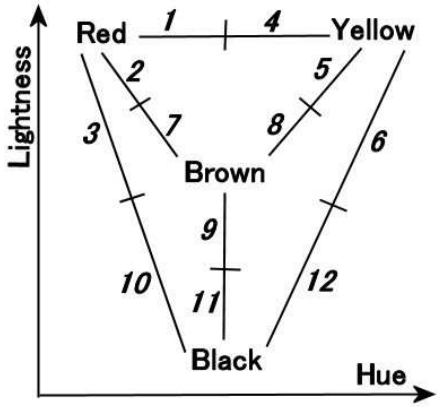

Fig. 16 The relation diagram among four background colors

According to Table VII, the lightness can distinguish hemorrhages from dust artifacts in any of the four states.

TABLE VII
EFFECTIVENESS EVALUATION OF LIGHTNESS

Four states	Red			Yellow			Brown			Black		
	1	2	3	4	5	6	7	8	9	10	11	12
Black spots	T	T		T	T		T	T				
White spots	T	T	T	T	T	T	T	T	T	T	T	T

According to Table Ⅷ, the saturation possibly had different capabilities for each color. If the background color is yellow, saturation can make the distinction, but not for black spots. In contrast, if the background color is black, saturation can make the distinction only for white spots. If the background color is red or brown, distinguishing the spots on the basis of saturation will be difficult.

TABLE VIII
EFFECTIVENESS EVALUATION OF SATURATION

Four states	Red			Yellow			Brown			Black		
	1	2	3	4	5	6	7	8	9	10	11	12
Black spots	F	F		F	F		F	F				
White spots	F	F	F	M	M	T	F	F	F	M	M	T

TABLE IX
EFFECTIVENESS EVALUATION OF HUE

Four states	Red			Yellow			Brown			Black		
	1	2	3	4	5	6	7	8	9	10	11	12
Black spots	T	M		T	M		F	F				
White spots	T	M	T	T	M	T	F	F	F	T	M	T

As seen in Table Ⅸ, for each color, hue has different capabilities for distinguishing hemorrhages from the dust artifacts. If the background color is red, yellow, or black, hue

can make the distinction. If the background color is brown, distinguishing the spots on the basis of hue will be difficult.

B. Photographing the artificial eye

We constructed the experimental device that can photograph artificial eyes. The fundus color of the artificial eye was ocher to resemble the fundus color of diabetic retinopathy. Each specimen was positioned on the central part and artificial eye side of the object lens and was photographed using the experimental device. When HLS color space was analyzed, lightness and saturation were found to be highly sensitive. However, hue was not highly sensitive. Using the experiment involving photography of the artificial eye, data about the eyeball could be obtained. Hence, this experiment was more important than the basic experiment using the magnifier and light bulbs. Further experiments involving changes in fundus color of the artificial eye will be performed in future. Moreover, the specimen size must be small to investigate the optimal size of house dust to be photographed.

VI. Conclusion

We investigated methods to distinguish small retinal hemorrhages in diabetic retinopathy from dust artifacts using HLS color space. Because an experiment to photograph a dust artifact was required, we constructed an experiment involving colored light bulbs and a magnifier. Dust artifacts were classified into two categories: black spots and white spots. Background colors were red, yellow, brown, and black. In HLS color space, lightness could distinguish hemorrhages from dust artifacts under all conditions; however, hue and saturation could distinguish hemorrhages from dust artifacts only under some conditions.

Furthermore, we constructed an experimental device that can photograph artificial eyes. The experimental device photographed the dust artifact using the artificial eye with an ocherous fundus. Lightness and saturation were found to be highly sensitive. However, hue was not highly sensitive.
These methods can automatically distinguish small hemorrhages from dust artifacts using lightness and saturation.

Acknowledgment

Photographs from diabetic retinopathy patients were provided by Hiroshima University Hospital. For research expenses, the intramural budget of Hiroshima International University was used. We are very thankful to all those who helped in our research.

References

[1] O. T. Tsuchiya., Measure Against Lifestyle Related Disease, JMAJ, Vol.49 no.3, 2006, pp132-134.
[2] E. Duh, Diabetic Retinopathy, Humana Press, 2008, pp29-66
[3] American Diabetes Association, Diabetic retinopathy, Clinical Diabetes, Vol. 19, No. 1, 2001, pp29-32
[4] S. S. Savant and H. B. Chandalia, Diabetic retinopathy, Intnl. J. Dev. Contries, Vol. 10, 1991, pp,9-25
[5] J. B. Brown, K. L. Pedula, K. H. Summers, Diabetic retinopathy, Diabetes Care, Vol. 26, No. 9, 2003, pp2637-2642.
[6] S. Garg and R. M. Davis, Diabetic retinopathy screening update, Clinical diabetes, Vo. 27, No. 4, 2009, pp140-145.
[7] I. U. Scott, N. M. Bressler, S. B. Bresseler et al, Agreement between clinical and reading center gradings of diabetic retinopathy severity level at baseline in a phase 2 study of intravitreal bevacizumab for diabetic macular edema, Retina, Vol. 28, No. 1, 2008, pp36-40.
[8] M. S. Figueroa, I . Contreras, S. Noval, Anti-angiogetic drugs as an adjunctive therapy in the surgical treatment of diabetic retinopathy, Curr Diabetes Rev., Vol. 5, No. 1, 2009, pp52-56.
[9] A.G. Oomen, J. P. C. M. Janssen, A. Dusseldorp et al., Ecposure to chemicals via house dust, RIVM Report 609021064/2008, 2008, pp11-18.
[10] E. Fernández-Caldas, W. L. Trudeau and D. K. Ledford, Environmental control of indoor biologic agents. J. Allergy. Clin. Immunol., issue 2, part 2, 1994, pp404-412.
[11] R. G. Willson, M. W. Maimone, A. E. Johnson et al, An Optical Model for Image Artifacts Produced by Dust Particles on Lenses, Proc. ISAIRAS 2005 Conference, 2005, ESA SP p603.
[12] A.V. Shukla, Clinical Optics Primer for Ophthalmic Medical Personnel, A Guide to Laws, Formulae, Calculations, and Clinical Applications, SLACK Inc. 2009, pp85-89.
[13] M. Born and E. Wolf, Principles of Optics 7th expanded edition, Electromagnetic Theory of Propagation, Interference and Diffraction of Light, Cambridge Univ. Press, 1999, pp142-227.
[14] D. D. David, R. Prescott, and S. Kennedy, Simultaneous stereoscopic fundus camera incorporating a single optical axis, Invest. Ophthalmol. Vis. Sci. March, 1980, pp289-297.
[15] R. Zeimer, S. Zou, T. Meeder et al, A fundus camera dedicated to the screening of diabetic retinopathy in the primary-care physician's office, IOVS May, Vol. 43, No. 5, 2002, pp1581-1587
[16] M. Niemeijer, B. Ginneken, S. R. Russell et al, Automated detection and differential of drusen, exudates, and cotton-wool spots in digital color fundus photographs for diabetic retinopathy diagnosis, Invest. Ophthalmol. Vis. Sci., Vol. 48, No. 5, 2007, pp2260-2267.
[17] D.Y. Lin, M. S. Blumenkrans, R. J. Brothers et al, The sensitivity and specificity of single-field nonmydriatic monochromatic digital fundus photography with remote image interpretation for diabetic retinopathy screening: a comparison with ophthalmoscopy and standardized mydriatic color photography, Am. J. Ophthalmol., Vol. 134, 2002, pp204-213.
[18] J. A. Olson, F. M. Strachan, J. H. Hipwell et al, A comparative evaluation of digital imaging, retinal photography and optometrist examination in screening for diabetic retinopathy, Diabet. Med., Vol. 20, 2003, pp528-534.
[19] A. E. Dirik, H. T. Sencar and N. Memon, Source Camera Identification Based on Sensor dust Characteristics, Signal Processing Applications for Public Security and Forensics 2007, SAFE'07, IEEE Workshop, 2007, pp1-6.
[20] R. Bergman, R. Maurer, H. Nachlieli et al, Comprehensive Solutions for Removal of Dust and Scratches from Images, Journal of Electronic Imaging, Vol. 17, No. 1, 2008, pp1-25.
[21] A. Zamfir, A. Drimbarean, M. Zamfir et al., An Optic Model of the Appearance of Blemishes in Digital Photographs, Proceedings of SPIE, Vol. 6502, Digital Photography 3, 2007.
[22] A. E. Dirik, H. T. Sencar and N. Memon, Digital Single Lens Reflex Camera Identification From Traces of Sensor Dust, IEEE Trans. Info. For. and Sec., Vol. 3, No. 3, 2008, pp539-552.
[23] R. F. Lyon, Prism-Based Color Separation for Professional Digital Photography, Proceedings of IS&T's PICS 2000 Conference: Image Processing, Image Quality, Image Capture Systems Conference, Oregon, 2000, pp50-54.
[24] H. Narasimha-Iyer, A. Can, B. Roysam et al., Robust Detection and Classification of Longitudinal Changes in Color Retinal Fundus Images for Monitoring Diabetic Retinopathy, IEEE Trans. Biomed. Eng., Vol. 53, No. 6, 2006, pp1084-1098.
[25] H. Narasima-lyer, A. Can, B. Roysam et al, Integrated analysis of vascular and nonvascular changes from color retinal fundus image sequences., IEEE Trans Biomed Eng., Vol. 54, No. 8, 2007, pp1436-45.
[26] P. J. Saine, Errors in Fundus Photography, Journal of Ophthalmic Photography, Vol. 7, No. 2, 1984, pp120-122.

[27] M. Tkalˇciˇc & F. J. Tasiˇc, Colour spaces – perceptual , historical and applicational background, EUROCON 2003, Computer as a tool, The IEEE Region 8, Vol.1, 2003, pp304-308.
[28] J. Koenderink, Colour for the sciences, The MIT Press, 2009, pp45-52, pp497-537.
[29] B. Jahne, Practical Handbook on Image Processing for Scientific Applications, CRC Press, 1997, pp102-107.
[30] B. G. Haskell, A. Puri and A. N. Netravali, Digital Video: An Introduction to MPEG-2, Chapman & Hall, 1997, pp86-91.
[31] A. Hanbury and J. Serra, Mathematical Morphology in the HLS Colour Space, 12th British Machine Vision Conference, Manchester, UK, 2001, pp 451–460.
[32] Jasc Software, Inc., Chapter 8: Making color and Tonal Corrections, Paint Shop Pro 8 User Guide, 2002, pp181-206.
[33] R. A. Peters II, Mathematical morphology for angle-valued images, Proceedings of the SPIE, Nonlinear Image Processing VIII 3026, 1997, pp84-94.
[34] Nikon Corporations, Nikon D1X Operators Manual, pp212-219.
[35] FUJIFILM Corporation, Digital Camera FinePix J27/J28/J29/J30/J32/J37/J38 Owner's Manual, pp99-104.
[36] Canon Inc., Canon EOS 50D Instruction Manual, pp204-210, 2008

Naoto Suzuki is earned the necessary credits, but before receiving Ph.D., he left the doctoral course in Graduate School of Engineering, The University of Tokyo, in 2000. He researched on an ophthalmologic device while working with a medical device maker and received Ph.D. from Chiba University in 2007. Since 2009, he has been an assistant professor in Hiroshima International University.